$pp \to pK^+\Lambda$ reaction in an effective Lagrangian model

R. Shyam*
Saha Institute of Nuclear Physics, Calcutta 700064, India

(Received 15 January 1999; revised manuscript received 16 July 1999; published 20 October 1999)

We investigate the $pp \to pK^+\Lambda$ reaction within an effective Lagrangian model where the contributions to the amplitudes are taken into account within the tree level. The initial interaction between the two nucleons is modeled by the exchange of π, ρ, ω, and σ mesons, and the ΛK^+ production proceeds via the excitation of the $N^*(1650)$, $N^*(1710)$, and $N^*(1720)$ baryonic resonances. The parameters of the model at the nucleon-nucleon-meson vertices are determined by fitting the elastic nucleon-nucleon scattering with an effective interaction based on the exchange of these four mesons, while those at the resonance vertices are calculated from the known decay widths of the resonances as well as the vector meson dominance model. Available experimental data is described well by this approach. The one-pion-exchange diagram dominates the production process at both higher and lower beam energies. The ρ and ω meson exchanges make negligible contributions. However, the σ-exchange processes contribute substantially to the total cross sections at lower beam energies. The excitation of the $N^*(1710)$ and $N^*(1650)$ resonances dominate this reaction at beam momenta above and below 3 GeV/c, respectively. The interference among the amplitudes of various resonance excitation processes is significant. For beam energies very close to the K^+ production threshold the hyperon-proton final state interaction effects are quite important. The data is selective about the model used to describe the low-energy scattering of the two final state baryons. [S0556-2813(99)02211-6]

PACS number(s): 25.40.Ve, 11.80.−m, 13.75.Cs, 13.75.Ev

I. INTRODUCTION

In recent years there has been a considerable amount of interest in the study of the associated production reaction $p+p \to p+K^+ +\Lambda$. This is expected to provide information on the manifestation of quantum chromodynamics (QCD) in the nonperturbative regime of energies larger than those of the low-energy pion physics where the low-energy theorem and partial conservation of axial current (PCAC) constraints provide a useful insight into the relevant physics [1]. The strangeness quantum number introduced by this reaction leads to new degrees of freedom into this domain which are expected to probe the admixture of $\overline{ss}$ quark pairs in the nucleon wave function [2] and also the hyperon-nucleon and hyperon-strange-meson interactions [3,4].

The elementary nucleon-nucleon-strange-meson production cross sections are the most important ingredients in the transport model studies of the K^+-meson production in the nucleus-nucleus collisions, which provide information on not only the initial collision dynamics but also the nuclear equation of state at high density [5–12]. Furthermore, the enhancement in the strangeness production has been proposed as a signature for the formation of the quark-gluon plasma in high-energy nucleus-nucleus collisions [13,14].

The experimental data on the $pp \to pK^+\Lambda$ reaction is very scarce. The measurements performed in late 1960's and 1970's provide total cross sections for this reaction at beam momenta larger than 2.80 GeV/c (see, e.g., [15]). With the advent of the high-duty proton-synchrotron, cooler synchrotron (COSY) at the Forschungszentrum, Jülich, it has become possible to perform systematic studies of the associated strangeness production at beam momenta very close to the reaction threshold (2.340 GeV/c). The first round of experiments at COSY have already added [16] 12 new data points to the data base. At near-threshold beam energies the final state interaction effects among the outgoing particles are significant. Therefore, the new set of data are expected to also probe the hyperon-nucleon and hyperon-strange meson interactions, along with the mechanism of the strangeness production in proton-proton collisions.

The existing theoretical studies of this reaction are based either on a single boson (π or K meson) exchange mechanism [17–20] or a resonance model [21–24]. In the first method, the K^+ production is assumed to take place essentially through the exchange of one intermediate pion or K-meson; the excitation of any intermediate nucleon resonance is not considered. The K-meson exchange amplitudes were found to dominate [17,20] the production cross sections. However, the relative sign of the pion and K-meson exchange amplitudes was not fixed in this approach [20]. Furthermore, it has been argued that the existing high energy data can be well reproduced considering only the single pion-exchange process [18,19] since the contribution of the K-meson exchange amplitude can be compensated by various parameters of the model.

In the resonance model [21] of the strangeness production in pp collisions, the π-, η-, and ρ-meson exchanges are included and the K^+-meson production proceeds via the excitation of the $N^*(1650)$, $N^*(1710)$, and $N^*(1720)$ resonances [22,24]. However, the terms in the total amplitude involving the interference of various resonance contributions are neglected in these calculations. Moreover, the parameters of the $NN\pi$ and $NN\rho$ vertices were taken from the Bonn nucleon-nucleon potential which may not be adequate at higher beam energies as these have been determined by fit-

*Electronic address: shyam@tnp.saha.ernet.in

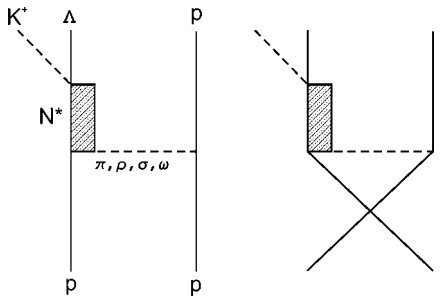

FIG. 1. Feynman diagrams for $K^+\Lambda$ production in pp collisions. The diagram on the left shows the direct process, while that on the right shows the exchange one.

ting the NN scattering data below the $NN\pi$ production threshold. At the same time, the finite lifetime of the ρ meson has not been taken into account while calculating the relevant coupling constants from the experimental branching ratios.

In this paper, we investigate the associated K^+ production in the proton-proton collisions in the framework of an effective Lagrangian approach [25–29], following and extending our previous study [30,31] on π^0 and π^+ production. Initial interaction between two incoming nucleons is modeled by an effective Lagrangian which is based on the exchange of the π, ρ, ω, and σ mesons. The coupling constants at the nucleon-nucleon-meson vertices are determined by directly fitting the T matrices of the nucleon-nucleon (NN) scattering in the relevant energy region [33]. The effective-Lagrangian uses the pseudovector (PV) coupling for the nucleon-nucleon-pion vertex (unlike the resonance model [22]), and thus incorporates the low-energy theorems [34] of current algebra and the hypothesis of partially conserved axial-vector current (PCAC). The K^+ production proceeds via excitation of the $N^*(1650)$, $N^*(1710)$, and $N^*(1720)$ intermediate baryonic resonance states which have appreciable branching ratios for the decay into the $K^+\Lambda$ channel. The interference terms between various intermediate resonance states are included which marks a major difference between our work and the resonance model [22]. To describe the recent near threshold data, the final state interaction between the outgoing particles is included within the framework of the Watson-Migdal theory [31].

The remainder of this paper is organized in the following way. Section II contains details of our theoretical approach. Section III comprises the results of our analysis and their critical discussion. The summary and conclusions of our work are presented in Sec. IV.

II. FORMALISM

We consider the tree-level structure (Fig. 1) of the amplitudes for the associated $K^+\Lambda$ production in proton-proton collisions, which proceeds via the excitation of the $N^*(1650)$ $(\frac{1}{2}^-)$, $N^*(1710)$ $(\frac{1}{2}^+)$, and $N^*(1720)$ $(\frac{3}{2}^+)$ intermediate resonances. To evaluate these amplitudes within the effective Lagrangian approach, one needs to know the effective Lagrangians (and the coupling constants appearing therein) at (i) nucleon-nucleon-meson, (ii) resonance-nucleon-meson, and (iii) resonance-K^+-hyperon vertices. These are discussed in the following subsections.

A. Nucleon-nucleon-meson vertex

The parameters for NN vertices are determined by fitting the NN elastic scattering T matrix with an effective NN interaction based on the π, ρ, ω, and σ meson exchanges. The effective meson-NN Lagrangians are

$$\mathcal{L}_{NN\pi} = -\frac{g_{NN\pi}}{2m_N}\bar{\Psi}_N\gamma_5\gamma_\mu\boldsymbol{\tau}\cdot(\partial^\mu\boldsymbol{\Phi}_\pi)\Psi_N, \tag{1}$$

$$\mathcal{L}_{NN\rho} = -g_{NN\rho}\bar{\Psi}_N\left(\gamma_\mu + \frac{k_\rho}{2m_N}\sigma_{\mu\nu}\partial^\nu\right)\boldsymbol{\tau}\cdot\boldsymbol{\rho}^\mu\Psi_N, \tag{2}$$

$$\mathcal{L}_{NN\omega} = -g_{NN\omega}\bar{\Psi}_N\left(\gamma_\mu + \frac{k_\omega}{2m_N}\sigma_{\mu\nu}\partial^\nu\right)\omega^\mu\Psi_N, \tag{3}$$

$$\mathcal{L}_{NN\sigma} = g_{NN\sigma}\bar{\Psi}_N\sigma\Psi_N. \tag{4}$$

In Eqs. (2) and (3) $\sigma_{\mu\nu}$ is defined as

$$\sigma_{\mu\nu} = \frac{i}{2}(\gamma_\mu\gamma_\nu - \gamma_\nu\gamma_\mu). \tag{5}$$

We have used the notations and conventions of Bjorken and Drell [32]. In Eq. (1) m_N denotes the nucleon mass. It should be noted that we have used a PV coupling for the $NN\pi$ vertex. Since we use these Lagrangians to directly model the T matrix, we have also included a nucleon-nucleon-axial-vector-isovector vertex, with the effective Lagrangian given by

$$\mathcal{L}_{NNA} = g_{NNA}\bar{\Psi}\gamma_5\gamma_\mu\boldsymbol{\tau}\Psi\cdot\mathbf{A}^\mu, \tag{6}$$

where A represents the axial-vector meson field. This term is introduced because in the limit of large axial meson mass (m_A) it cures the unphysical behavior in the angular distribution of NN scattering caused by the contact term in the one-pion exchange amplitude [33], if g_{NNA} is chosen to be

$$g_{NNA} = \frac{1}{\sqrt{3}}m_A\left(\frac{f_\pi}{m_\pi}\right), \tag{7}$$

with very large $(\gg m_N)$ m_A. f_π appearing in Eq. (7) is related to $g_{NN\pi}$ as $f_\pi = (g_{NN\pi}/2m_N)m_\pi$.

It should be mentioned here that the contact term of the coordinate space potential, corresponding to one pion exchange term, is effectively switched off by the repulsive hard core of the nucleon-nucleon interaction. However, in the effective Lagrangian description, this term has to be explicitly subtracted in order to avoid the unphysical behavior of the elastic cross section. This is achieved by the inclusion of a term corresponding to the exchange of a axial-vector-isovector meson as described above.

We introduce, at each interaction vertex, the form factor

TABLE I. Coupling constants for the NN-meson vertices used in the calculations.

Meson	$g^2/4\pi$	l	λ (GeV)	mass (GeV)
π	12.562	0.1133	1.005	0.138
σ	2.340	0.1070	1.952	0.550
ω	46.035	0.0985	0.984	0.783
ρ	0.317	0.1800	1.607	0.770

$k_\rho = 6.033,\ k_\omega = 0.0$

$$F_i^{NN} = \left(\frac{\lambda_i^2 - m_i^2}{\lambda_i^2 - q_i^2} \right), \quad i = \pi, \rho, \sigma, \omega, \tag{8}$$

where q_i and m_i are the four momentum and mass of the ith exchanged meson, respectively. The form factors suppress the contributions of high momenta and the parameter λ_i, which governs the range of suppression, can be related to the hadron size. Since NN elastic scattering cross sections decrease gradually with the beam energy (beyond certain value), we take energy dependent meson-nucleon coupling constants of the following form:

$$g(\sqrt{s}) = g_0 \exp(-l\sqrt{s}), \tag{9}$$

in order to reproduce these data in the entire range of beam energies. The parameters g_0, λ, and l were determined by fitting to the elastic proton-proton and proton-neutron scattering data at the beam energies in the range of 400 MeV–4.0 GeV [30,33]. It may be noted that this procedure also fixes the sign of the effective Lagrangians [Eqs. (1)–(4), (6)]. The values of various parameters are shown in Table I [the signs of all the coupling constants (g) are positive], which are the same as those used in the calculations of the pion production in proton-proton collisions [30,31]. Thus we ensure that the NN elastic scattering channel remains the same in the description of various inelastic channels within this approach, as it should be.

B. Resonance-nucleon-meson vertex

As the Λ hyperon has zero isospin, only isospin-1/2 nucleon resonances are allowed. Below 2 GeV center of mass (c.m.) energy, only three resonances, $N^*(1650)$, $N^*(1710)$, and $N^*(1720)$, have significant decay branching ratios (3–11 %, 5–25 %, and 1–15 %, respectively [35]) into the $K^+\Lambda$ channel. In this work only these three resonances have been considered. The $N^*(1700)$ resonance having very small (and uncertain) branching ratio for the decay to this channel has been excluded.

Since all of the three resonances can couple to the meson-nucleon channel considered in the previous section, we require the effective Lagrangians for all of the four resonance-nucleon-meson vertices corresponding to all of the included resonances. For the coupling of the spin-1/2 resonances to pion we again have the choice of pseudoscalar (PS) or PV couplings. The corresponding effective Lagrangians can be written as [29,36,37]

$$\mathcal{L}^{PV}_{N^*_{1/2}N\pi} = -\frac{g_{N^*_{1/2}N\pi}}{M} \bar{\Psi}_{N^*} \Gamma_\mu \boldsymbol{\tau} \cdot (\partial^\mu \boldsymbol{\Phi}_\pi) \Psi_N + \text{H.c.}, \tag{10}$$

$$\mathcal{L}^{PS}_{N^*_{1/2}N\pi} = -g_{N^*_{1/2}N\pi} \bar{\Psi}_{N^*} i\Gamma \boldsymbol{\tau} \boldsymbol{\Phi}_\pi \Psi_N + \text{H.c.}, \tag{11}$$

where $M = (m_{N^*} \pm m_N)$, with the upper sign for even parity and lower sign for odd parity resonance. The operators Γ, Γ_μ are given by

$$\Gamma = \gamma_5, \quad \Gamma_\mu = \gamma_5 \gamma_\mu, \tag{12}$$

$$\Gamma = 1, \quad \Gamma_\mu = \gamma_\mu, \tag{13}$$

for resonances of even and odd parities, respectively. We have performed calculations with both of these couplings. The effective Lagrangians for the coupling of resonances to other mesons are similar to those given by Eqs. (2)–(4),

$$\mathcal{L}_{N^*_{1/2}N\rho} = -g_{N^*_{1/2}N\rho} \bar{\Psi}_{N^*} \frac{1}{2m_N} \Gamma_{\mu\nu} \partial^\nu \boldsymbol{\tau} \cdot \boldsymbol{\rho}^\mu \Psi_N + \text{H.c.}, \tag{14}$$

$$\mathcal{L}_{N^*_{1/2}N\omega} = -g_{N^*_{1/2}N\omega} \bar{\Psi}_{N^*} \frac{1}{2m_N} \Gamma_{\mu\nu} \partial^\nu \omega^\mu \Psi_N + \text{H.c.}, \tag{15}$$

$$\mathcal{L}_{N^*_{1/2}N\sigma} = g_{N^*_{1/2}N\sigma} \bar{\Psi}_{N^*} \Gamma' \sigma \Psi_N + \text{H.c.} \tag{16}$$

The operators Γ' and $\Gamma_{\mu\nu}$ are

$$\Gamma' = 1, \quad \Gamma_{\mu\nu} = \sigma_{\mu\nu}, \tag{17}$$

$$\Gamma' = \gamma_5, \quad \Gamma_{\mu\nu} = \gamma_5 \sigma_{\mu\nu} \tag{18}$$

for resonances of even and odd parities, respectively.

The even parity isospin-1/2 $N^*(1720)$ resonance is a spin-3/2 nucleon excited state. We have used the following effective Lagrangians for vertices involving this resonance [29,36,37]:

$$\mathcal{L}_{N^*N\pi} = \frac{g_{N^*_{3/2}N\pi}}{m_\pi} \bar{\Psi}_\mu \boldsymbol{\tau} \cdot \partial^\mu \boldsymbol{\Phi}_\pi \Psi_N + \text{H.c.}, \tag{19}$$

$$\mathcal{L}_{N^*N\rho} = i\frac{g_{N^*_{3/2}N\rho}}{m_{N^*} + m_N} \bar{\Psi}_\mu \boldsymbol{\tau} (\partial^\nu \boldsymbol{\rho}^\mu - \partial^\mu \boldsymbol{\rho}^\nu) \gamma_\nu \gamma_5 \Psi_N + \text{H.c.}, \tag{20}$$

$$\mathcal{L}_{N^*N\omega} = i\frac{g_{N^*_{3/2}N\omega}}{m_{N^*} + m_N} \bar{\Psi}_\mu \boldsymbol{\tau} (\partial^\nu \omega^\mu - \partial^\mu \omega^\nu) \gamma_\nu \gamma_5 \Psi_N + \text{H.c.}, \tag{21}$$

$$\mathcal{L}_{N^*N\sigma} = \frac{g_{N^*_{3/2}N\sigma}}{m_\sigma} \bar{\Psi}_\mu \boldsymbol{\tau} \cdot (\partial^\mu \sigma) \Psi_N + \text{H.c.}, \tag{22}$$

Here $\bar{\Psi}_\mu$ is the $N^*(1720)$ vector spinor. It should be remarked here that an operator $\Theta_{\alpha\mu}(z)=g_{\alpha\nu}-\frac{1}{2}(1+2z)\gamma_\alpha\gamma_\mu$ has also been included in the vector spinor vertex in Refs. [29,36,37]. This operator describes the off-shell admixture of the spin-1/2 fields [38]. The choice of the off-shell parameter z is arbitrary and it is treated as a free parameter to be determined by fitting to the data. This operator can be easily introduced in Eqs. (19)–(22) which will introduce four additional free parameters in our calculations. We however, work with the Lagrangians as given in Eqs. (19)–(22), which are identical to those given in [29,36,37] for $z=0.5$.

C. Resonance-hyperon-strange-meson vertex

For vertices involving spin-1/2 resonances, there is again the PS and PV coupling option. In principle, one can select a linear combination of both and fit the PS/PV ratio to the data. However, to minimize the number of parameters we choose either PS or PV coupling at a time. The effective Lagrangians for the $N^*\Lambda K^+$ vertex is written in the following way [36,37].

For spin-1/2 resonance,

$$\mathcal{L}^{PV}_{N^*_{1/2}\Lambda K^+}=-\frac{g_{N^*_{1/2}\Lambda K^+}}{M'}\bar{\Psi}_{N^*}\Gamma_\mu\boldsymbol{\tau}\cdot(\partial^\mu\boldsymbol{\Phi}_{K^+})\Psi_N+\text{H.c.}, \tag{23}$$

$$\mathcal{L}^{PS}_{N^*_{1/2}\Lambda K^+}=-g_{N^*_{1/2}\Lambda K^+}\bar{\Psi}_{N^*}i\Gamma\boldsymbol{\tau}\boldsymbol{\Phi}_{K^+}\Psi_N+\text{H.c.}, \tag{24}$$

where $M'=m_{N^*}\pm m_\Lambda$, with the upper sign for even parity and lower sign for odd parity resonance.

For spin-3/2 resonance,

$$\mathcal{L}_{N^*_{3/2}\Lambda K^+}=\frac{g_{N^*_{3/2}\Lambda K^+}}{m_{K^+}}\bar{\Psi}_\mu\boldsymbol{\tau}\cdot\partial^\mu\boldsymbol{\Phi}_{K^+}\Psi_N+\text{H.c.} \tag{25}$$

D. Coupling constants for resonances

The resonance couplings are determined from the experimentally observed quantities, such as the branching ratios for the decay of the resonances to the corresponding channels. The partial width for the decay of a resonance (in its rest frame) of mass M_{N^*} into a meson of mass m_m and energy E_m, and a nucleon is written in terms of the Lorenz invariant matrix element $\mathcal{M}$ as

$$d\Gamma=\frac{(2\pi)^4}{2M_{N^*}}|\mathcal{M}|^2\delta^4(P_{N^*}-p_m-p_N)\frac{d^3p_m}{(2\pi)^3 2E_m}\frac{m_N}{E_N}\frac{d^3p_N}{(2\pi)^3}. \tag{26}$$

In the case of the meson (in the decay channel) having a finite lifetime for the decay to another channel (e.g., $\rho\to\pi\pi$), an integration over the phasespace for this decay must be included [39–41].

1. $N^*N\pi$ vertex

For the spin-1/2 resonance, the $N^*N\pi$ decay width, with the PS coupling, is given by

$$\Gamma_{N^*_{1/2}N\pi}=\frac{3}{4\pi}g^2_{N^*_{1/2}N\pi}\frac{E_N\pm m_N}{m_{N^*}}p^{cm}_\pi, \tag{27}$$

while that with the corresponding PV coupling is

$$\Gamma_{N^*_{1/2}N\pi}=\frac{3}{4\pi}\left(\frac{g_{N^*_{1/2}N\pi}}{M}\right)^2\left[\frac{2E_\pi[E_NE_\pi+(p^{cm}_\pi)^2]-m^2_\pi(E_N\pm m_N)}{m_{N^*}}\right]p^{cm}_\pi, \tag{28}$$

where

$$p^{cm}_\pi=\frac{[m^2_{N^*}-(m_N+m_\pi)^2][m^2_{N^*}-(m_N-m_\pi)^2]}{4m^2_{N^*}}, \tag{29}$$

$$E_N=\sqrt{(p^{cm}_\pi)^2+m^2_N}, \tag{30}$$

$$E_\pi=\sqrt{(p^{cm}_\pi)^2+m^2_\pi}. \tag{31}$$

For spin-3/2 resonance, the $N^*N\pi$ decay width is

$$\Gamma_{N^*_{3/2}N\pi}=\frac{1}{12\pi}\left(\frac{g_{N^*_{3/2}N\pi}}{m_\pi}\right)^2\frac{E_N\pm m_N}{m^*_N}(p^{cm}_\pi)^3. \tag{32}$$

The plus and minus sign in Eqs. (27) corresponds to odd and even parity resonances, respectively, while in Eqs. (28) and (32), the reverse is the case.

2. $N^*N\rho$ vertex

The partial decay width of each resonance for the decay into nucleon and two pions via the ρ meson is given by

$$\Gamma(m_{N^*})=2\int_{2m_\pi}^{m_{N^*}-m_N}dm\,m\Gamma^*(m)S(m). \tag{33}$$

In this equation the spectral function $S(m)$ is defined as

$$S(m)=-\frac{1}{\pi}ImD_\rho(m), \tag{34}$$

where

$$D_\rho(m) = \frac{1}{m^2 - m_\rho^2 + im\Gamma_{\rho\to\pi\pi}}, \tag{35}$$

with

$$\Gamma_{\rho\to\pi\pi} = \Gamma^0_{\rho\to\pi\pi}\frac{m_\rho^2}{m^2}\left[\frac{p_{\rho\pi\pi}(m)}{p_{\rho\pi\pi}(m_\rho)}\right]^3. \tag{36}$$

The value of $\Gamma^0_{\rho\to\pi\pi}$ is taken to be 150 MeV. The $\rho\to\pi\pi$ decay four-momenta $p_{\rho\pi\pi}$ are

$$p_{\rho\pi\pi}(m) = \frac{[m^2 - 4m_\pi^2][m^2]}{4m^2}. \tag{37}$$

In Eq. (33), $\Gamma^*(m)$ is defined in the following way. For spin-1/2 even parity resonance,

$$\Gamma^*(m) = \frac{1}{4\pi}\left(\frac{g_{N^*_{1/2}N\rho}}{2m_N}\right)^2 \times\left[\frac{4(E_N^*+E_m)(p_m^{cm})^2 + 3(E_N^*-m_N)m^2}{m_{N^*}}\right]p_m^{cm}, \tag{38}$$

$$E_N^* = \sqrt{(p_m^{cm})^2 + m_N^2}, \tag{39}$$

$$E_m = \sqrt{(p_m^{cm})^2 + m^2}, \tag{40}$$

where p_m^{cm} is given in the same way as Eq. (29) with m_π replaced by m.
For spin-1/2 odd parity resonance,

$$\Gamma^*(m) = \frac{1}{4\pi}\left(\frac{g_{N^*_{1/2}N\rho}}{2m_N}\right)^2 \times\left[\frac{-4(E_N^*+E_m)(p_m^{cm})^2 - 3(E_N^*+m_N)m^2}{m_{N^*}}\right]p_m^{cm}. \tag{41}$$

For spin-3/2 even parity resonance,

$$\Gamma^*(m) = \frac{1}{12\pi}\left(\frac{g_{N^*_{3/2}N\rho}}{m_{N^*}+m_N}\right)^2 \times\left[\frac{2(2E_N^*+E_m)(p_m^{cm})^2 + 3(E_N^*-m_N)m^2}{m_{N^*}}\right]p_m^{cm}. \tag{42}$$

3. $N^*N\omega$ vertex

Since the resonances considered in this study have no known branching ratios for the decay into the $N\omega$ channel, we determine the coupling constants for the $N^*N\omega$ vertices by the strict vector meson dominance (VMD) hypothesis [42], which is based essentially on the assumption that the coupling of photons on hadrons takes place through a vector meson.

The $N^*N\gamma$ partial widths are given as the following. For spin-1/2 even parity resonance,

$$\Gamma_{N^*N\gamma} = \frac{1}{\pi}\frac{m_N}{m_{N^*}}(\mu_{N^*})^2(q_f^3). \tag{43}$$

For spin-1/2 odd parity resonance,

$$\Gamma_{N^*N\gamma} = \frac{3}{2}\frac{m_N}{m_{N^*}}(\mu_{N^*})^2\left(m_N^2 + \frac{2}{3}q_f^2\right)q_f. \tag{44}$$

For spin-3/2 even parity resonance,

$$\Gamma_{N^*N\gamma} = \frac{1}{\pi}\frac{m_N}{m_{N^*}}(\mu_{N^*})^2(q_f^3). \tag{45}$$

In these equations, $q_f = [(m_{N^*}^2 - m_N^2)/2m_{N^*}]$. The value of μ_{N^*} is determined by fitting to the $N\gamma$ partial width of each resonance, which is given in terms of the helicity amplitudes $A_{1/2}$ and $A_{3/2}$ by [35]

$$\Gamma_\gamma = \frac{q_f^2}{\pi}\frac{2m_N}{(2J+1)m_{N^*}}[|A_{1/2}|^2 + |A_{3/2}|^2], \tag{46}$$

where J is the resonance spin. μ_{N^*} is written as the ratio of the couplings at $N^*\omega$ and $\omega\gamma$ vertices as

$$\mu_{N^*} = e\frac{g_{N^*\omega}}{g_{\omega\gamma}}. \tag{47}$$

Using the above equations together with the experimental helicity amplitudes, the values of the coupling constants for the $N^*N\omega$ vertices can be determined. We have used $g_{\omega\gamma} = 17$ in our calculations.

4. $N^*N\sigma$ vertex

As the sigma meson is, most of the time, a resonance of two pions [43] in the S state, the coupling constants for the $N^*N\sigma$ vertices are determined from the branching ratios of the decay of the resonances into $N(\pi\pi)^{I=0}$. We, however, reduce the experimental values of these ratios by 2/3 to account for the fact that this correlated state provides only about 2/3 of the total 2π exchange. The expressions for the partial widths are similar to those given by Eqs. (27)–(32).

5. $N^*\Lambda K^+$ vertex

The coupling constants for the $N^*\Lambda K^+$ vertices are determined from the experimental branching ratios for the $N^* \to \Lambda K^+$ decay. The expressions for the decay widths are similar to those given by Eqs. (27)–(32).

We assume that the off-shell dependence of the NN^* vertices are determined solely by multiplying the vertex constants by the form factors, which have the dipole form [30,44]

TABLE II. Coupling constants and cutoff parameters for the N^*N-meson and N^*-hyperon-meson vertices used in the calculations.

Resonance	Width (GeV)	Decay channel	Adopted value of the branching ratio	$g^2/4\pi$	λ^{N^*} (GeV)
$N^*(1710)$	0.100	$N\pi$	0.150	0.0863	0.850
		$N\rho$	0.150	1.3653	0.850
		$N\omega$		0.1189	0.850
		$N\sigma$	0.170	0.0361	0.850
		ΛK	0.150	2.9761	0.850
$N^*(1720)$	0.150	$N\pi$	0.100	0.0023	0.850
		$N\rho$	0.700	90.637	0.850
		$N\omega$		22.810	0.850
		$N\sigma$	0.120	0.1926	0.850
		ΛK	0.080	0.0817	0.850
$N^*(1650)$	0.150	$N\pi$	0.700	0.0521	0.850
		$N\rho$	0.08	0.5447	0.850
		$N\omega$		0.2582	0.850
		$N\sigma$	0.025	0.2882	0.850
		ΛK	0.070	0.0485	0.850

$$F_i^{NN^*}=\left(\frac{(\lambda_i^{N^*})^2-m_i^2}{(\lambda_i^{N^*})^2-q_i^2}\right)^2, \quad i=\pi,\rho,\sigma,\omega. \tag{48}$$

The resonance properties used in the calculations of the decay widths are given in Table II, where the resulting coupling constants and the adopted values of the cutoff parameters ($\lambda_i^{N^*}$) are also given. It may be noted that we have fixed the latter to one value in order to minimize the number of free parameters.

It should, however, be stressed that the branching ratios determine only the square of the corresponding coupling constants; thus their signs remain uncertain in this method. Predictions from independent calculations (e.g., the quark model) can, however, be used to constrain these signs. The magnitude, as well signs of the coupling constants for the $N^*N\pi$, $N^*\Lambda K$, $N^*N\rho$, and $N^*N(\pi\pi)_{s\text{-}wave}$ vertices were determined by Feuster and Mosel [37], and Manley and Saleski [45] in their analysis of the pion-nucleon data involving the final states πN, $\pi\pi N$, ηN, and $K\Lambda$. Predictions for some of these quantities are also given in the constituent quark model calculations of Capstick and Roberts [46]. Guided by the results of these studies, we have chosen the positive sign for the coupling constants for these vertices. Unfortunately, quark model calculations for the $N^*N\omega$ vertices are still sparse and an unambiguous prediction for the signs of the corresponding coupling constants may not be possible at this stage [47]. Nevertheless, we have chosen a positive sign for the coupling constants for these vertices as well.

E. Propagators

We require the propagators for various mesons and nucleon resonances in the calculation of the amplitudes. The propagators for pion, ρ-meson, and axial-vector mesons are given by

$$G_\pi(q)=\frac{i}{(q^2-m_\pi^2)}, \tag{49}$$

$$G_\rho^{\mu\nu}(q)=-i\left(\frac{g^{\mu\nu}-q^\mu q^\nu/q^2}{q^2-m_\rho^2}\right), \tag{50}$$

$$G_A^{\mu\nu}(q)=-i\left(\frac{g^{\mu\nu}}{q^2-m_A^2}\right). \tag{51}$$

In Eq. (51), the mass of the axial meson is taken to be very large (188 GeV), since the corresponding amplitude is that of the contact term. The propagators for ω and σ mesons are similar to those given by Eqs. (50) and (49), respectively.

The propagators for spin-1/2 and spin-3/2 resonances are

$$G_{N^*_{1/2}}(p)=i\left(\frac{p\!\!\!/+m_{N^*_{1/2}}}{p^2-[m_{N^*_{1/2}}-i(\Gamma_{N^*_{1/2}}/2)]^2}\right), \tag{52}$$

$$G^{\mu\nu}_{N^*_{3/2}}(p)=-\frac{i(p\!\!\!/+m_{N^*_{3/2}})}{p^2-[m_{N^*_{3/2}}-i(\Gamma_{N^*_{3/2}}/2)]^2}\left[g^{\mu\nu}-\frac{1}{3}\gamma^\mu\gamma^\nu-\frac{2}{3m^2_{N^*_{3/2}}}p^\mu p^\nu+\frac{1}{3m^2_{N^*_{3/2}}}(p^\mu\gamma^\nu-p^\nu\gamma^\mu)\right]. \tag{53}$$

In Eqs. (52) and (53), Γ_{N^*} is the total width of the resonance, which is introduced in the denominator term $(p^2-m^2_{N^*})$ to account for the fact that the resonances are not the stable particles; they have a finite lifetime for the decay into various channels. Γ_{N^*} is a function of the center-of-mass momentum of the decay channel, and it is taken to be the sum of the widths for pion and rho decay (the other decay channels are considered only implicitly by adding their branching ratios to that of the pion channel):

$$\Gamma_{N^*}=\Gamma_{N^*\to N\pi}+\Gamma_{N^*\to N\rho}. \tag{54}$$

$\Gamma_{N^*\to N\rho}$ is calculated according to Eq. (33). $\Gamma_{N^*\to N\pi}$ is taken to be

$$\Gamma_{N^*\to N\pi}=\Gamma_0\left(\frac{p^{cm}_{\pi R}}{p^{cm}_\pi}\right)^{2l+1}, \tag{55}$$

where l is the orbital angular momentum of the resonance. p^{cm}_π is as defined in Eq. (29) and $p^{cm}_{\pi R}$ is given by the same equation with m_{N^*} replaced by p of Eqs. (52) and (53). Γ_0 is taken to be the total on-shell width of the resonance minus the corresponding width for the nucleon-ρ meson decay channel.

F. Amplitudes and cross sections

After having established the effective Lagrangians, coupling constants, and form of the propagators, we can now proceed to calculate the amplitudes for various diagrams as-

sociated with the $pp \to p\Lambda K^+$ reaction. These amplitudes can be written by following the well-known Feynman rules [48] and calculated numerically by following, e.g., the techniques discussed in [30]. The isospin part is treated separately. This gives rise to a constant factor for each graph, which is unity for the reaction under study. It should be stressed here that signs of various amplitudes are fixed by those of the effective Lagrangians, coupling constants, and the propagators as described above. These signs are not allowed to change anywhere in the calculations.

The general formula for the invariant cross section of the $p+p \to p+\Lambda+K^+$ reaction is written as

$$d\sigma = \frac{m_N^3 m_\Lambda}{2\sqrt{[(p_1p_2)^2 - m_N^4]}} \frac{1}{(2\pi)^5} \delta^4(P_f - P_i) |A_{fi}|^2 \prod_{a=1}^{3} \frac{d^3p_a}{E_a}, \tag{56}$$

where A_{fi} represents the total amplitude, P_i and P_f, the sum of all the momenta in the initial and final states, respectively, and p_a, the momenta of the three particles in the final state. The corresponding cross sections in the laboratory or center-of-mass systems can be written from this equation by imposing the relevant conditions.

G. Final state interaction

For describing the data for the $pp \to p\Lambda K^+$, reaction at beam energies very close to the threshold, consideration of the final state interaction (FSI) among the three outgoing particles is important. As there exists no theory of the FSI effects in the presence of three strongly interacting particles, we follow an approximate scheme in line exactly with the Watson-Migdal theory of FSI [49]. In this approach the energy dependence of the cross section due to FSI is separated from that of the primary production amplitude. This method has been applied earlier to study the low-momentum behavior of the η meson [50] and pion spectra [51,31,52] measured in proton-proton collisions. We write for the total amplitude

$$A_{fi} = M_{fi}(pp \to p\Lambda K^+) T_{ff}, \tag{57}$$

where $M_{fi}(pp \to p\Lambda K^+)$ is the primary production amplitude as discussed above, while T_{ff} describes the rescattering among the final particles, which goes to unity in the limit of no FSI. The latter is taken to be the coherent sum of the two-body on-mass-shell elastic scattering amplitudes of the particles involved in the final channel:

$$T_{ff} = \sum_{i=1}^{3} t_i^{l_i}(q_i), \tag{58}$$

where t_i represents the two-body on-shell elastic scattering amplitude (of the interacting particles pair j-k) in the three-body space with the ith particle being the spectator. l_i and q_i denote the partial wave and relative momentum of the j-k particle pair, respectively.

An assumption inherent in the approximation given by Eq. (57) is that the reaction takes place over a small region of space, a condition fulfilled rather well in near-threshold reactions involving heavy mesons. This allows us to express the amplitudes t_i in terms of the inverse of the Jost function, $J_{l_i}(q_i)$ [53,31]. In the analysis presented in this paper we assume $l_i = 0$, for all of the three pairs j-k and use the modified Cini-Fubini-Stanghellini formula [54] for the effective range expansion of the phase shift (δ_{0i}) of the relevant pair

$$C_0^2 q_i \cot \delta_{0i} + 2q_i \eta h(\eta) = (1/a_i) + (1/2) r_{0i} q_i^2 \tag{59}$$

to calculate the corresponding Jost function. It may be noted that in the case of the pair j-k involving uncharged particle(s), the second term on the left-hand side of Eq. (59) vanishes and C_0^2 goes to unity. In this equation, r_{0i} and a_i are the effective range and scattering length parameters, respectively, for the j-k interacting pair. η is the corresponding Coulomb parameter and

$$C_0^2 = \frac{2\pi\eta}{e^{2\pi\eta} - 1}, \quad h(\eta) = \sum_{n=1}^{\infty} \frac{\eta^2}{n(n^2+\eta^2)} - 0.5772 - \ln(\eta). \tag{60}$$

In this case we have

$$t_i^0(q_i) = [J_0(q_i)]^{-1} = \frac{(q_i^2 + \alpha_i^2) r_{0i}^c/2}{1/a_i^c + (r_{0i}^c/2) q_i^2 - i q_i}, \tag{61}$$

where α is given by

$$\alpha = (1/r_{0i}^c)[1 + (1 + 2r_{0i}^c/a_i^c)^{1/2}] \tag{62}$$

and a_i^c and r_{0i}^c are defined as

$$\frac{1}{a_i^c} = \frac{1}{C_0^2}\left[\frac{1}{a_i} - 2q_i \eta h(\eta)\right], \tag{63}$$

$$r_{0i}^c = \frac{r_{0i}}{C_0^2}. \tag{64}$$

It may be noted that for large q_i, the amplitude t_i goes to unity, which is to be expected. The extrapolation of the scattering amplitude for the off-shell effects can be achieved by means of a monopole form factor [20]. For a detailed discussion of the off-shell effects we refer to [55].

The factorization of the total amplitude into those of the FSI and primary production [Eq. (57)], enables one to pursue the diagrammatic approach for the latter within an effective Lagrangian model and investigate the role of various meson exchanges and resonances in describing the reaction. Moreover, in this way the FSI among all of the three outgoing particles can be included. Although the meson-baryon interactions are weak, they can still be influential through interference.

The parameters a and r_0 are very poorly known for the K^+-nucleon and K^+-hyperon systems, since the corresponding scattering data are scarce at low energies. On the other hand, for the hyperon-nucleon system, several sets of values for these parameters have been given by the Bonn-Jülich

TABLE III. Scattering length (a) and effective range (r_0) parameters for the ΛN scattering derived from models A, $\tilde{A}$, B, and $\tilde{B}$ of the Jülich-Bonn group [56] and D, F, and NSC of the Nijmegen group [57].

Model	a(singlet) (fm)	r_0(singlet) (fm)	a(triplet) (fm)	r_0(triplet) (fm)
A	1.56	1.43	1.59	3.16
$\tilde{A}$	2.04	0.64	1.33	3.91
B	0.56	7.77	1.91	2.43
$\tilde{B}$	0.40	12.28	2.12	2.57
D	1.90	3.72	1.96	3.24
F	2.29	3.17	1.88	3.36
NSC	2.78	2.88	1.41	3.11

[56] and Nijmegen [57] groups from their respective $\Lambda-p$ interaction models. There is quite some variation in the values given in these sets. For the K^+-p and $K^+-\Lambda$ systems we have adopted the values given in a recent effective Lagrangian model analysis of the available $K\Lambda$ and Kp data by Feuster and Mosel [37]. In any case, the cross sections are insensitive to the FSI effects in these channels. On the other hand, these effects are very important in the $\Lambda-p$ channel and we have performed calculations of the corresponding FSI effects with all of the sets of these parameters given by Bonn-Jülich and Nijmegen groups (given in Table III) in order to see if the results are sensitive to various models. More details will be given in the next section.

III. RESULTS AND DISCUSSION

The theoretical approach presented in the previous section has been used to study the available data on the $p+p\rightarrow p+\Lambda+K^+$ reaction for beam energies ranging from just above the production threshold to about 10 GeV. In the results shown below, we have used PS couplings for both $N^*N\pi$ and $N^*\Lambda K^+$ vertices involving spin-1/2 resonances of even and odd parities. However, calculations have also been performed with the corresponding PV couplings. The cross sections calculated with this option for the resonance-hyperon-kaon vertex deviate very little from those obtained with the corresponding PS couplings. However, the PV coupling for the $N^*N\pi$ vertex leads to noticeably different results as is discussed below.

A. Cross-section data for beam energy above 2 GeV

In Fig. 2 we show the comparison of our calculations with the experimental data for the total cross section for this reaction as a function of beam momentum for incident energies above 2 GeV. In this figure we have investigated the role of various meson exchange processes in describing the total cross section. The dotted, dashed, long-dashed, and dashed-dotted curves represent the contributions of π, ρ, ω, and σ meson exchanges, respectively. The contribution of the heavy axial meson exchange is not shown in this figure since it is negligibly small. The coherent sum of all of the meson-exchange processes is shown by the solid line. The experimental points are taken from [15]. We note that the measured cross sections are reproduced reasonably well by our calculations (solid line) for all of the beam energies except for the two lowest points. The FSI effects, which are not included in these calculations, reduce the discrepancy between the experimental data and calculations at these beam momenta. This point is further discussed in the next subsection.

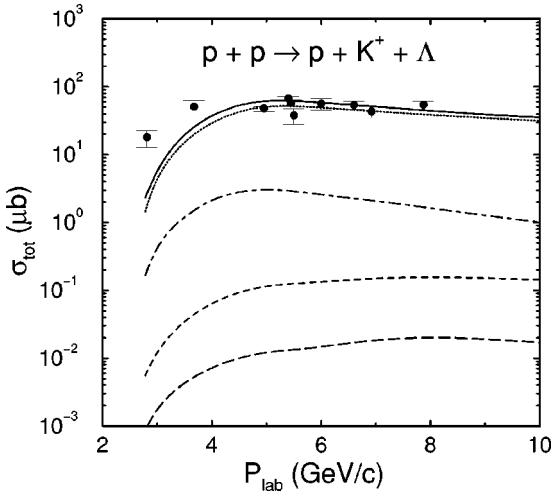

FIG. 2. Total cross section for the $p+p\rightarrow p+K^+ +\Lambda$ reaction as a function of the beam momentum. The dotted, dashed, long-dashed, and dashed-dotted curves represent the contributions of π, ρ, ω, and σ meson exchanges, respectively. Their coherent sum is shown by the solid line. The experimental data are from [15].

We note that the pion exchange graphs dominate the production process for all of the energies. In comparison to this, the contributions of ρ and ω meson exchanges are almost insignificant. The ρ-meson exchange, which is a convenient way of taking into account the P wave part of the correlated two-pion exchange (CTPE) process, is rather weak even in the low-energy NN scattering [43]. With increasing projectile energy, its contribution decreases further. On the other hand, the σ meson exchange, which models the CTPE in the $\pi\pi$ S wave and provides about 2/3 of this exchange in the low-energy NN interaction, plays a relatively more important role. This observation has also been made in the case of the $NN\rightarrow NN\pi$ reaction [58–60,30,31]. Thus, the σ meson exchange provides an efficient means of mediating the large momentum mismatch involved in the meson production reactions in NN collisions, particularly at lower beam momenta.

The relative importance of the contributions of each intermediate resonance to the $pp\rightarrow p\Lambda K^+$ reaction is studied in Fig. 3, where the contributions of $N^*(1650)$, $N^*(1710)$, and $N^*(1720)$ resonances to the energy dependence of the total cross section are shown by dotted, dashed, and dashed-dotted lines, respectively. Their coherent sum is depicted by the solid line. It is clear that the contributions from the $N^*(1710)$ and $N^*(1650)$ resonances dominate the total cross section at beam momenta above and below 3 GeV/c, respectively. Moreover, the interference terms of the amplitudes corresponding to various resonances are quite important. This result is in sharp contrast to the resonance model

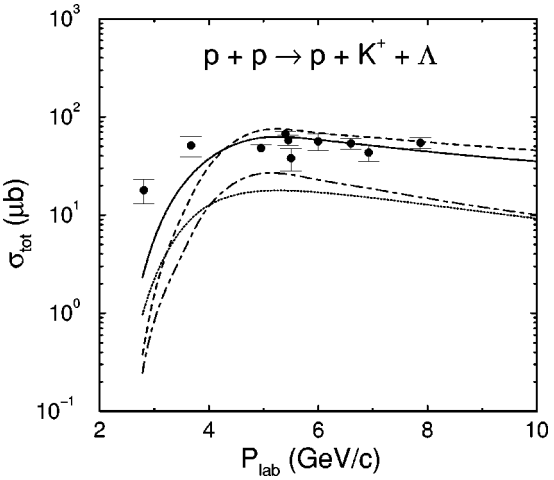

FIG. 3. Contributions of $N^*(1650)$ (dotted line), $N^*(1710)$ (dashed line), and $N^*(1720)$ (dashed-dotted line) baryonic resonances to the total cross section for the $p+p \to p+K^+ + \Lambda$ reaction as a function of beam momentum. Their coherent sum is shown by the solid line.

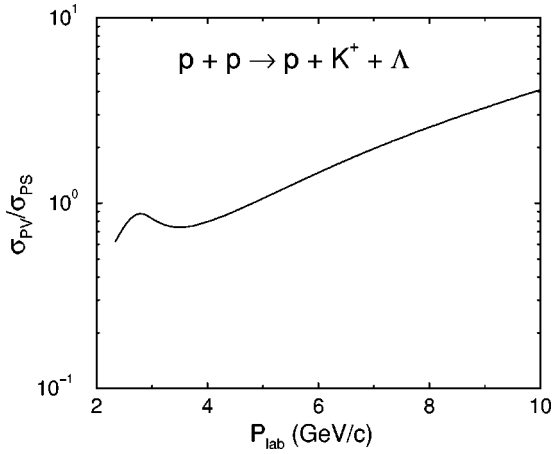

FIG. 4. Ratio of the total cross section calculated with pseudovector and pseudoscalar couplings for the $N^*N\pi$ vertex corresponding to spin-1/2 (even and odd parity) resonance for the same reaction as in Fig. 2, as a function of beam momentum.

calculations of Refs. [21,22,24], where these terms were ignored. It must again be emphasized that we have no freedom in choosing the relative signs of the interference terms.

Looking at Table II, one might naively expect the dominance of the $N^*(1710)$ resonance everywhere as the coupling constants for the $N^*\Lambda K^+$ and $N^*N\pi$ vertices for the $N^*(1710)$ resonance are about an order of magnitude larger than those for $N^*(1720)$ and $N^*(1650)$ resonances. In fact, the relative importance of various resonances is determined by the dynamics of the reaction mechanism. As the beam energy rises above the K^+ production threshold, the excitation of the resonance lowest in energy is more probable in the beginning. However, with increasing beam energy the excitation of the higher-energy resonances starts playing a more and more important role.

As mentioned earlier, the use of the PV coupling for the $N^*\Lambda K$ vertices (involving spin-1/2 even and odd parity resonances) makes insignificant changes in the cross sections. However, there is a clear preference for the PS coupling at the $N^*N\pi$ vertices. This is shown in Fig. 4, where the ratio of the total cross section, obtained by using the PV (σ_{PV}) and PS (σ_{PS}) couplings for these vertices, is shown as a function of the beam momentum. It is seen that σ_{PV} is larger than σ_{PS} at higher beam momenta, while at lower ones the reverse is true. Clearly, PS coupling for the $N^*N\pi$ vertex provides a better description of the beam energy dependence of the total cross section for the $pp \to pK^+\Lambda$ reaction.

B. Cross-section data for beam energies below 2 GeV

In Fig. 5 we compare the results of our calculations (with FSI effects included) with the recent data [16] for the $pp \to pK^+\Lambda$ reactions at beam energies very close to the kaon production threshold. In this figure the total cross section is shown as a function of the excess energy $(\epsilon) = \sqrt{s} - m_N - m_{K^+} - m_\Lambda$, where $\sqrt{s}$ is the invariant mass. The FSI effects were included by following the procedure outlined in Sec. II G. We have chosen [37] $a = 0.065 + i0.040$, $r_0 = -15.930 - i8.252$, and $a = -0.214$, $r_0 = -0.331$ for the $K^+\Lambda$ and K^+p systems, respectively, in all of the calculations shown below. For the $\Lambda - p$ system all of the seven sets of the parameters as shown in Table III were used.

In Fig. 5(a), the results obtained with the parameter sets of models *A* (dotted line), $\tilde{A}$ (solid line), *B* (dashed line), and $\tilde{B}$ (long-dashed-dotted line) of the Bonn-Jülich group [56] are

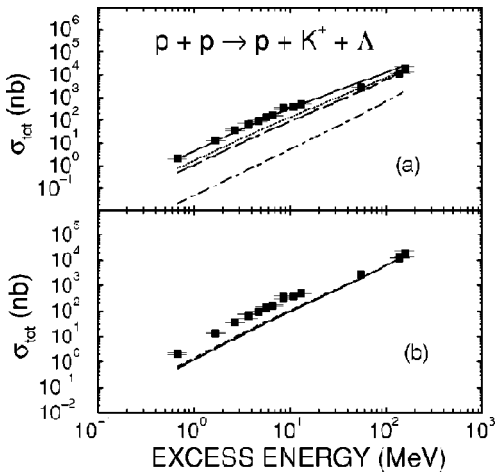

FIG. 5. Total cross section for the $p+p \to p+K^+ + \Lambda$ reaction very close to the K^+ production threshold as a function of the excess energy (defined in the text). The FSI effects are included by using the scattering length (a) and effective range (r_0) parameters for the $K^+ - \Lambda$ and $K^+ - p$ systems taken from the Ref. [37] and those for the $\Lambda - p$ system from the sets given by Jülich-Bonn [56] and Nijmegen [57] groups. In the upper part (a), results obtained with the $\Lambda - p$ parameters of models *A* (dotted line), $\tilde{A}$ (solid line), *B* (dashed line), and $\tilde{B}$ (long-dashed line) of the former group are shown, while in the lower part (b), those of models *D*, *F*, and NSC of the latter group are depicted. Results of the three models of the Nijmegen group are indistinguishable from each other. In the upper part (a), results with no FSI effects are shown by dashed-dotted line. The experimental data are taken from [15,16].

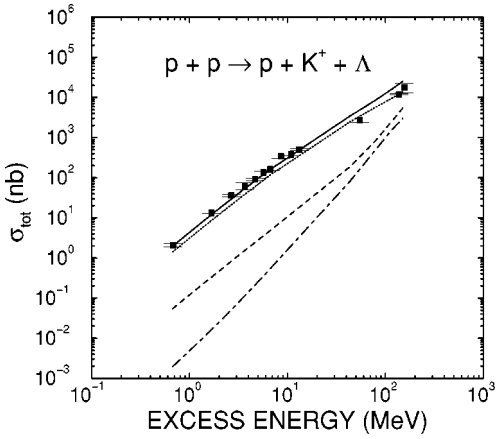

FIG. 6. Contributions of $N^*(1650)$ (dotted line), $N^*(1710)$ (dashed line), and $N^*(1720)$ (dashed-dotted line) baryonic resonances to the total cross section for the same reaction as in Fig. 5, as a function of the excess energy. Their coherent sum is shown by the solid line. The FSI effects are included with a and r_0 parameters of the K^+-p and $K^+-\Lambda$ systems being the same as those in Fig. 5 and those for the $\Lambda-p$ system being taken from model $\tilde{A}$ of the Jülich-Bonn group [56]. The experimental data are from [16,15].

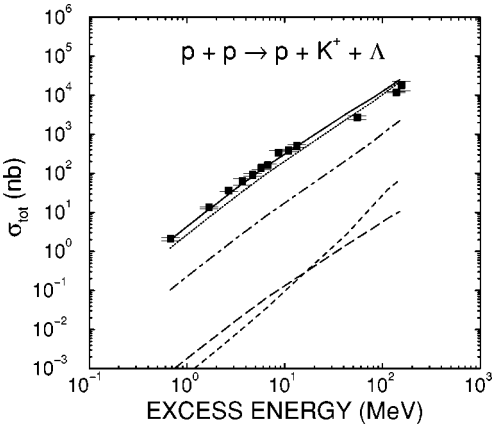

FIG. 7. Contributions of π (dotted line), ρ (dashed line), ω (long-dashed line), and σ (dashed-dotted line) meson exchange processes to the total cross section for the same reaction as shown in Fig. 6, as a function of the excess energy. Their coherent sum is shown by the solid line. The FSI effects are included in the same way as in Fig. 6. The experimental data are from [16,15].

shown. It can be noted that all four models provide similar results for the total cross sections at $\epsilon \sim 150$ MeV. However, at lower values of ϵ, the cross sections calculated with models A and $\tilde{A}$ are larger than those of models B and $\tilde{B}$ by a factor of about 2–3. Moreover, there is a difference of a factor of more than 2 between the results obtained with model A and $\tilde{A}$ itself with the latter providing a better overall agreement with the data. We also show in this figure the results obtained without including the FSI effects (dashed-dotted line). It can be noted that the FSI effects are quite important in order to describe the experimental data.

The results obtained with models D, E, and NSC of the Nijmegen group [57] are shown in Fig. 5(b). These three models produce almost identical results for all values of ϵ. However, while the data at the higher excess energies are reproduced by all three models quite well, they underpredict the cross sections at lower ϵ by a factor of about 3. Therefore, while all of the models of the $\Lambda-p$ interaction (considered in this work) provide an equally good description of the total cross section data at higher values of the excess energy, a difference of factors of 2–3 occurs between their predictions at lower values of ϵ. Thus, the near-threshold ΛK^+ production data in proton-proton collisions are sensitive to the S-wave Λ-nucleon interaction and may be used to distinguish between various models proposed in the literature to describe this interaction. We note that model $\tilde{A}$ of the Bonn-Jülich group provides the best overall description of the data, which has been used to account for the $\Lambda-p$ FSI effects in all of the calculations discussed subsequently.

The individual contributions of various nucleon resonances to the total cross section of the $pp \rightarrow p\Lambda K^+$ reaction near the production threshold is shown in Fig. 6 as a function of the excess energy. In contrast to the situation at higher beam energies ($p_{lab} \geqslant 3$ GeV/c), the cross section is dominated by the $N^*(1650)$ resonance excitation. This is in line with the observations made in Refs. [23,24]. It may, however, be noted that in Ref. [24], the FSI effects have not been included and no comparison with the data at near-threshold energies is shown.

Since $N^*(1650)$ is the lowest-energy baryonic resonance having an appreciable branching ratio for the decay to the ΛK^+ channel, its dominance in this reaction at beam energies near the kaon production threshold is to be expected. The contributions of the other two resonances $[N^*(1710)$ and $N^*(1720)]$ are several orders of magnitude smaller, therefore, the resonance-resonance interference terms are also very small. Thus, near threshold energies, this reaction proceeds preferentially via excitation of the $N^*(1650)$ resonance. It may be noted that in Ref. [24], the FSI effects have not been included in these calculations.

In Fig. 7, we show the contributions of various meson exchanges to this reaction at near-threshold beam energies. Various curves have the same meaning as in Fig. 2. The one-pion exchange graphs dominate the reaction in this energy regime as well. On the other hand, the individual contributions of the ρ and ω meson exchange processes are negligible. However, those of the σ meson exchange are substantial in this energy regime. Thus, as near-threshold pion production in proton-proton collisions, the heavy scalar meson exchange plays an important role in this case too. It should be noted, however, that the interference terms of various meson exchange processes are not negligible; contributions of various exchange processes simply do not add up to the total cross section obtained by the coherent addition of various amplitudes.

IV. SUMMARY AND CONCLUSIONS

We investigated the associated $K^+\Lambda$ production in the proton-proton collisions at energies ranging from near threshold to about 10 GeV. This reaction is of interest since it provides the prospect of testing QCD in the nonperturbative domain at energies larger than the pion mass. In this

paper our goal has been to investigate this reaction within an effective Lagrangian model, which is proven to be very successful in describing the pion production in NN collisions. Most of the parameters of this model are fixed by fitting to the elastic NN T matrix; this restricts the freedom of varying the parameters of the model to provide a fit to the data. The reaction proceeds via the excitation of the $N^*(1650)$, $N^*(1710)$, and $N^*(1720)$ intermediate nucleon resonant states. The coupling constants at vertices involving resonances have been determined from the experimental branching ratios of their decay into various relevant channels. Unlike the $NN\pi$ vertex, there is no compelling reason to choose the pseudovector (PV) form for the $N^*\Lambda K^+$ and $N^*N\pi$ couplings (involving spin-1/2 resonances of even and odd parities) and we investigated both the PV and pseudoscalar (PS) couplings at these vertices. To describe the data at the near-threshold beam energies, we have included the FSI effects among the outgoing particles by following the Watson-Migdal theory, which has been used before successfully to describe the $NN\eta$ and $NN\pi$ reactions in the similar energy regimes.

With the same set of parameters, the model is able to provide a good description of the data at higher, as well as near threshold beam energies. The one-pion-exchange processes make the dominant contribution to the cross section in the entire energy regime. The individual contributions of the ρ and ω meson exchange diagrams are very small every where. Although, the interference terms of their amplitudes with those of other meson exchanges may still be noticeable. On the other hand, the σ exchange makes a relatively larger contribution at lower beam energies, confirming the earlier observation that the heavy scalar meson provides a means of mediating the large momentum transfer in near-threshold NN-meson production processes.

While at beam momenta larger than 3 GeV/c, the reaction proceeds predominantly via excitation of the $N^*(1710)$ resonance, the process gets maximum contribution from the $N^*(1650)$ resonance at lower beam energies. A very striking feature of our results is that the interference among various resonance contributions is significant. Therefore, in the calculations of this reaction, these terms should not be ignored.

The near-threshold data clearly favors the excitation of the $N^*(1650)$ resonance. Therefore, this reaction, in this energy regime, provides an ideal means of investigating the properties of this baryonic resonance.

Unlike the $NN\pi$ vertex where there is a clear preference for the PV coupling, as seen in the $NN\pi$ data, the present reaction does not distinguish between PS and PV couplings at the $N^*\Lambda K^+$ vertex involving spin-1/2 even or odd parity resonance. However, the PS coupling at the $N^*N\pi$ vertex is clearly favored by the data.

The near-threshold data may be selective about the model describing the low-energy Λ-nucleon scattering. Calculations of the FSI effects performed with the scattering length and effective range parameters of the Jülich-Bonn group produce different results as compared to those performed with the corresponding parameters of the Nijmegen group. The parameters of model $\tilde{A}$ of Ref. [56] provide the best agreement with the data.

An obvious extension of the present work is to calculate the cross sections for the $pp \to p\Sigma K^+$ reaction, for which the measurements have recently been performed at COSY [61]. This will also lead to the inclusive K^+ cross sections in the elementary nucleon-nucleon collisions which are the necessary input to the transport model calculations of the strangeness production in the heavy ion collisions. This work is currently underway by extending the model to include the excitation of delta isobars $\Delta(1910)$ and $\Delta(1920)$ which are four star and three star resonances, respectively. Since the on-shell $N^*(1650) \to \Sigma K$ decay is not allowed, techniques similar to those described in Sec. II D 2 will have to be used to calculate the coupling constant for this vertex. It would also be interesting to calculate the invariant mass spectrum of the hyperon K^+ pair which is expected to provide further information about the various resonance contributions to this reaction. This will be reported in a future publication. Extension of the present theory to incorporate the unitarity, perhaps on the lines of the K-matrix approximation [37], is also desirable.

ACKNOWLEDGMENTS

The author is thankful to Ulrich Mosel for his very kind hospitality at the University of Giessen during several visits and for numerous useful discussions which were very helpful in completing this work. He also wishes to thank Wolfgang Nörenberg and Jörn Knoll for their warm hospitality in the theory group of the GSI where a part of this work was done. Useful discussions with W. Cassing, B. Friman, G. Penner, W. Peters, M. Post, and A. Sibirtsev are gratefully acknowledged. Financial support from the Abdus Salam International Center for Theoretical Physics, Trieste, is thankfully acknowledged.

[1] T. E. O Ericson and W. Weise, *Pions and Nuclei* (Clarendon, Oxford, 1988).
[2] M. Alberg, Prog. Part. Nucl. Phys. **36**, 217 (1996).
[3] A. Deloff, Nucl. Phys. **A505**, 583 (1989).
[4] R. A. Adelseck and B. Saghai, Phys. Rev. C **42**, 108 (1990).
[5] U. Mosel, Annu. Rev. Nucl. Part. Sci. **41**, 29 (1991), and references therein.
[6] G. E. Brown, C. M. Ko, Z. G. Wu, and L. H. Xia, Phys. Rev. C **43**, 1881 (1991).
[7] T. Maruyama, W. Cassing, U. Mosel, S. Teis, and K. Weber, Nucl. Phys. **A573**, 653 (1994).
[8] D. Miskowiec *et al.*, Phys. Rev. Lett. **72**, 3650 (1994).
[9] C. Hartnack, J. Jaenicke, L. Sehn, H. Ströcker, and J. Aichelin, Nucl. Phys. **A580**, 643 (1994).
[10] X. S. Fang, C. M. Ko, G. Q. Li, and Y. M. Zheng, Nucl. Phys. **A575**, 766 (1994).

[11] G. Q. Li and C. M. Ko, Phys. Lett. B **349**, 405 (1995).
[12] G. Q. Li, C. M. Ko, and W. S. Chung, Phys. Rev. C **57**, 434 (1998).
[13] J. Rafelski and B. Müller, Phys. Rev. Lett. **48**, 1066 (1982).
[14] H. W. Barz, B. L. Friman, J. Knoll, and H. Schulz, Nucl. Phys. **A485**, 685 (1988).
[15] Landolt-Börnstein, *New Series*, edited by H. Schopper, I/12 (1988).
[16] J. T. Balewski *et al.*, Phys. Lett. B **388**, 859 (1996); **420**, 211 (1998); R. Bilger *et al.*, *ibid.* **420**, 217 (1998).
[17] E. Ferrari, Nuovo Cimento **15**, 652 (1960); E. Ferrari, Phys. Rev. **120**, 988 (1960).
[18] T. Yao, Phys. Rev. **125**, 1048 (1962).
[19] J. Q. Wu and C. M. Ko, Nucl. Phys. **A499**, 810 (1989).
[20] J. M. Laget, Phys. Lett. B **259**, 24 (1991).
[21] K. Tsushima, S. W. Huang, and Amand Faessler, Phys. Lett. B **337**, 245 (1994).
[22] K. Tsushima, A. Sibirtsev, and A. W. Thomas, Phys. Lett. B **390**, 29 (1997).
[23] G. Fäldt and C. Wilkin, Z. Phys. A **357**, 241 (1997).
[24] A. Sibirtsev, K. Tsushima, and A. W. Thomas, Phys. Lett. B **421**, 59 (1998).
[25] S. Weinberg, Phys. Rev. **166**, 1568 (1968).
[26] R. D. Peccei, Phys. Rev. **181**, 1902 (1969).
[27] R. M. Davidson, N. C. Mukhopadhyay, and R. S. Wittman, Phys. Rev. D **43**, 71 (1991).
[28] K. L. Hagalin, Ann. Phys. (N.Y.) **212**, 84 (1991).
[29] M. Benmerrouche, N. C. Mukhopadhyay, and J. F. Zhang, Phys. Rev. D **51**, 3237 (1995).
[30] A. Engel, R. Shyam, U. Mosel, and A. K. Dutt-Majumdaer, Nucl. Phys. **A603**, 387 (1996).
[31] R. Shyam and U. Mosel, Phys. Lett. B **426**, 1 (1998).
[32] J. D. Bjorken and S. D. Drell, *Relativistic Quantum Mechanics* (McGraw-Hill, New York, 1964).
[33] M. Schäfer, H. C. Dönges, A. Engel, and U. Mosel, Nucl. Phys. **A575**, 429 (1994).
[34] N. Dombay and B. J. Read, Nucl. Phys. **B60**, 65 (1973).
[35] Particle Data Group, C. Casso *et al.*, Eur. Phys. J. C **3**, 1 (1998).
[36] T. Feuster and U. Mosel, Nucl. Phys. **A612**, 375 (1997).
[37] T. Feuster and U. Mosel, Phys. Rev. C **58**, 457 (1998); T. Feuster (private communication).
[38] M. Benmerrouche, R. M. Davidson, and N. C. Mukhopadhyay, Phys. Rev. C **39**, 2339 (1989).
[39] B. Friman and H. J. Pirner, Nucl. Phys. **A617**, 496 (1997).
[40] R. Rapp, G. Chanfray, and J. Wambach, Nucl. Phys. **A617**, 472 (1997).
[41] W. Peters, M. Post, H. Lenske, S. Leupold, and U. Mosel, Nucl. Phys. **A632**, 109 (1998).
[42] J. J. Sakurai, *Currents and Mesons* (University of Chicago Press, Chicago, 1969); Ann. Phys. (N.Y.) **11**, 1 (1960).
[43] R. Machleidt, K. Hollinde, and Ch. Elster, Phys. Rep. **149**, 1 (1987).
[44] A. König and P. Kroll, Nucl. Phys. **A356**, 345 (1981).
[45] D. M. Manley and E. M. Saleski, Phys. Rev. D **45**, 4002 (1992).
[46] S. Capstick and W. Roberts, Phys. Rev. D **49**, 4570 (1994).
[47] Fl. Stancu and P. Stassart, Phys. Rev. D **47**, 2140 (1993).
[48] C. Itzykson and J. B. Zuber, *Quantum Field Theory* (McGraw-Hill, New York, 1964).
[49] K. M. Watson, Phys. Rev. **88**, 1163 (1952); A. B. Migdal, Zh. Éksp. Teor. Fiz. **28**, 3 (1955) [Sov. Phys. JETP **1**, 2 (1955)].
[50] A. Moalem, E. Gedalin, L. Razdolskaja, and Z. Shorer, Nucl. Phys. **A589**, 649 (1995); **A600**, 445 (1996).
[51] J. Dubach, W. M. Kloet, and R. R. Silbar, Phys. Rev. C **33**, 373 (1986).
[52] V. Bernard, N. Kaiser, and Ulf-G. Meissner, Eur. Phys. J. A **4**, 259 (1999).
[53] M. L. Goldberger and K. M. Watson, *Collision Theory* (Wiley, New York, 1969), p. 549.
[54] H. P. Noyes, Annu. Rev. Nucl. Sci. **22**, 465 (1972).
[55] C. Hanhart and K. Nakayama, Phys. Lett. B **454**, 176 (1999).
[56] A. Reuber, K. Hollinde, and J. Speth, Nucl. Phys. **A570**, 543 (1994).
[57] P. M. M. Maessen, T. A. Rijken, and J. J. de Swart, Phys. Rev. C **40**, 2226 (1989).
[58] V. Dmitriev, O. Sushkov, and C. Gaarde, Nucl. Phys. **A459**, 503 (1986).
[59] T. S. H. Lee and D. O. Riska, Phys. Rev. Lett. **70**, 2237 (1993).
[60] C. J. Horowitz, H. O. Meyer, and D. K. Griger, Phys. Rev. C **49**, 1337 (1994).
[61] S. Sewerin *et al.*, Phys. Rev. Lett. **83**, 682 (1999).